

An Improved Accuracy Split-Step Padé Parabolic Equation for Tropospheric Radio-Wave Propagation

Mikhail S. Lytaev(✉)

St. Petersburg Federal Research Center of the Russian Academy of Sciences, 14-th Linia, V.I., No. 39, Saint Petersburg 199178, Russia

Abstract. This paper is devoted to modeling the tropospheric electromagnetic waves propagation over irregular terrain by the higher-order finite-difference methods for the parabolic equation (PE). The proposed approach is based on the Padé rational approximations of the propagation operator, which is applied simultaneously along with longitudinal and transversal coordinates. At the same time, it is still possible to model the inhomogeneous tropospheric refractive index. Discrete dispersion analysis of the proposed scheme is carried out. A comparison with the other finite-difference methods for solving the parabolic equation and the split-step Fourier (SSF) method is given. It is shown that the proposed method allows using a more sparse computational grid than the existing finite-difference methods. This in turn results in more fast computations.

Keywords: Parabolic wave equation · Finite difference methods · Tropospheric propagation · Electromagnetic propagation · Numerical dispersion

1 Introduction

When solving several problems of wireless communications, navigation and radar, it is essential to predict the characteristics of radio-wave propagation in the constantly varying troposphere. The propagation of radio-waves is significantly affected by spatial variations in the tropospheric refractive index, irregular terrain and its dielectric properties, rough sea surface [9], vegetation [4,24], and urban development [16]. Often, the solution to this problem is an integral part of complex real-time software systems [3]. Given the above challenges, developing both appropriate mathematical models and efficient numerical methods remains actual.

The most widely used deterministic approach to solving this class of problems is the parabolic equation (PE) method [13,14]. Modern formulation of the PE method in terms of the one-way Helmholtz equation is directly derived from Maxwell's equations, which makes it rather reliable and verified. The PE method can take into account all the above-mentioned features of tropospheric propagation [9,10,23,28,29], but its effective usage requires fast and reliable numerical methods.

© Springer Nature Switzerland AG 2021
O. Gervasi et al. (Eds.): ICCSA 2021, LNCS 12949, pp. 418–433, 2021.
https://doi.org/10.1007/978-3-030-86653-2_31

The fastest and most widely used numerical method for solving the PE in tropospheric radio-wave propagation problems is the split-step Fourier (SSF) method [14,22]. Its main drawbacks include instability and errors when modeling the upper and lower boundary conditions [11,19]. Finite-difference methods for solving PE [1,5,19], in contrast, provide efficient boundary conditions modeling. However, the existing finite-difference methods for PE are more time-consuming. When performing numerical radio coverage predictions over rugged terrain or in urban canyons, it is necessary to account for large propagation angles, which requires a dense computational grid and a large approximation order [17]. This, in turn, leads to an increase in computational costs. A number of important results concerning the numerical solution of PE by the finite-difference methods were obtained in computational hydroacoustics studies [6]. The use of the principle of universality of mathematical models [25] makes it possible to partially reuse the corresponding numerical methods in the problem under consideration.

This article continues a series of works [17–19] devoted to improving the performance of finite-difference schemes for the PE. Previously, a higher-order approximation was applied along the longitudinal coordinate, while the diffraction part of the propagation operator was approximated by the 2nd or 4th order scheme. In this paper, it is shown that under certain conditions it is possible to simultaneously apply the higher-order Padé approximation to the exponential propagation operator and its diffraction part. At the same time, the new scheme differs only in coefficients, which means that it inherits all the properties of existing finite-difference schemes.

The paper is organized as follows. The next section presents a solution to the one-way Helmholtz equation using the split-step Padé method. In Sect. 3, we introduce a joint Padé approximation along with the longitudinal and transversal coordinates. Section 4 provides a comparative analysis of the numerical schemes under various propagation conditions.

2 Split-Step Padé PE

Following the generally accepted methodology of splitting the wave field into forward and backward propagating waves [8], the equation for waves propagating along the positive x direction can be written as follows

$$\frac{\partial u}{\partial x} = ik(\sqrt{1+L}-1)u, \tag{1}$$

where

$$Lu = \frac{1}{k^2}\frac{\partial^2 u}{\partial z^2} + hu,$$

$$h(x,z) = m^2(x,z) - 1,$$

$k = 2\pi/\lambda$ is the wavenumber, λ is the wavelength, $m(x,z)$ is the modified refractivity of the troposphere [14].

Function $u(x,z)$ is subject to the impedance boundary condition at the lower boundary

$$(q_1 u + q_2 \frac{\partial u}{\partial z})\Big|_{z=h(x)} = 0,$$

where $h(x)$ is the terrain profile, complex coefficients q_1 and q_2 are determined from the dielectric properties of the ground [14].

The wave propagation process is generated by the Dirichlet initial condition of the form

$$u(0,z) = u_0(z), \tag{2}$$

with known function $\psi_0(z)$, which corresponds to the antenna pattern.

Step-by-step solution of Eq. (1) can be formally written using the pseudo-differential [26] propagation operator as follows

$$u(x+\Delta x, z) = P(L)\, u(x,z), \tag{3}$$

$$P(L) = \exp\left(ik\Delta x\left(\sqrt{1+L}-1\right)\right).$$

The following notation is further used for discrete versions of functions

$$u_j^n = u(n\Delta x, j\Delta z),$$

where Δx and Δz are the longitudinal and transversal grid steps respectively.

Considering propagation operator (3) as a function of operator L, we can apply a rational Padé approximation of the order $[m/n]$ [2,5] as follows

$$P(L)\, u = \frac{1+\sum_{l=1}^{m} \tilde{a}_l L^l}{1+\sum_{l=1}^{n} \tilde{b}_l L^l} u + O(L^{n+m})u. \tag{4}$$

Next, we will represent the rational approximation in the form of a product

$$\frac{1+\sum_{l=1}^{m} \tilde{a}_l L^l}{1+\sum_{l=1}^{n} \prod \tilde{b}_l L^l} = \prod_{l=1}^{p} \frac{1+a_l L}{1+b_l L},$$

where $p = \max(m,n)$. The pseudo-differential square root operator, which is responsible for the diffraction, and the operator exponent, which is responsible for integration along the longitudinal coordinate x, are simultaneously approximated. Any desired propagation angle can be achieved by selecting a sufficient Padé approximation order [17].

The action of propagation operator (3) is approximately reduced to the sequential application of the rational operator of the form

$$v = \frac{1+a_l L}{1+b_l L} u,$$

which in turn is equivalent to solving the following one-dimensional differential equation

$$(1+bL)\, v = (1+aL)\, u, \tag{5}$$

where $u(z)$ is known field, obtained on a previous step, $v(z)$ is the desired field.

Replace operator L is Eq. (5) with its finite-difference analog [18]

$$\hat{L}u_j = \frac{1}{k^2\Delta z^2}\frac{\delta^2}{1+\alpha\delta^2} + h_j u_j,$$

where $\alpha = 0$ for the 2nd order approximation and $\alpha = 1/12$ for the 4th order approximation, second difference operator δ^2 is defined as follows

$$\delta^2 u = u(z-\Delta z) - 2u(z) + u(z+\Delta z) = u_{j-1} - 2u_j + u_{j+1}.$$

Then we obtain the following finite-difference equation

$$\begin{aligned}&\left(\tau\left(1+\alpha\delta^2\right) + b_l\delta^2 + b_l\tau h_j\right)v_j + b_l\tau\alpha\delta^2\left(h_j v_j\right)\\ &\quad = \left(\tau\left(1+\alpha\delta^2\right) + a_l\delta^2 + a_l\tau h_j\right)u_j + a_l\tau\alpha\delta^2\left(h_j u_j\right),\end{aligned}$$

where $\tau = (k\Delta z)^2$.

The above equation, along with discrete boundary conditions [18,19], is a tridiagonal system of linear algebraic equations and is solved in linear time. The result is a numerical scheme that has an arbitrary order of accuracy when integrated along the longitudinal coordinate x and up to 4th order accuracy in z.

Note that case $p = 1$ in approximation (4) is equivalent to the well known Crank-Nikolson scheme for PE [10]. At the same time, the Padé approximation scheme is significantly superior to the Crank-Nikolson method both in terms of computational speed and smoothness of the obtained solutions [14,19].

3 Modified Padé Approximation

A certain disadvantage of the previously obtained scheme is the approximation of transversal differentiation operator L. While an arbitrary order of accuracy is achievable for the approximation of the exponential operator, the order of approximation does not exceed 4 for operator L. It is reasonable to assume that increasing the approximation order of operator L can further improve the performance of the scheme. The obvious solution to this problem is the use of multi-point schemes for the approximation of the differential operator. However, it will also increase the complexity of the scheme, since Eq. (5) will no longer be reduced to a tridiagonal matrix. Instead, in this paper, we propose to use Padé approximation (4) simultaneously by the longitudinal and transversal coordinates.

Following [7,12], the differentiation operator can be expressed in terms of the second difference operator as follows

$$\frac{\partial^2 u}{\partial z^2} = g(\delta^2)u,$$

$$g(\xi) = -\frac{1}{\Delta z^2} \ln^2 \left(1 + \frac{\xi}{2} + \sqrt{\left(1 + \frac{\xi}{2}\right)^2 - 1} \right).$$

For the case of a homogeneous medium ($m(x, z) \equiv 1$) we can write down the following approximation of the propagation operator with respect to operator δ^2

$$P\left(\frac{1}{k^2}\frac{\partial^2}{\partial z^2}\right) u = P\left(\frac{1}{k^2} g\left(\delta^2\right)\right) u \approx \prod_{l=1}^{p} \frac{1 + a_l' \delta^2}{1 + b_l' \delta^2} u. \tag{6}$$

There is no explicit approximation of operator L in this expression. Thus, the longitudinal and transversal coordinate discretization is performed using single high-order Padé approximation. The disadvantage of this approach, which was previously considered for solving the computational hydroacoustics problems [5], is its limitation to the case of a homogeneous medium.

Let us now return to the case of an inhomogeneous troposphere. Function g is presented according to the Taylor series as follows

$$g(\xi) = \frac{1}{\Delta z^2} \left[\xi - \frac{1}{12}\xi^2 + \frac{1}{90}\xi^3 - \ldots \right].$$

Put $\delta^2 + \tau h$ as an argument of function g to the above decomposition

$$\begin{aligned} \frac{1}{k^2} g(\delta^2 + \tau h) u &= \frac{1}{\tau} \left[\delta^2 + \tau h - \frac{1}{12} \left(\delta^2 + \tau h\right)^2 + \frac{1}{90} \left(\delta^2 + \tau h\right)^3 - \ldots \right] u \\ &= \frac{1}{\tau} \left[\delta^2 u + \tau h u - \frac{1}{12} \left(\delta^4 u + \ldots\right) + \frac{1}{90} \left(\delta^6 u + \ldots\right) - \ldots \right]. \end{aligned}$$

In tropospheric propagation problems, $h(x, z)$ is a slowly varying function both in range and height, and its value rarely exceeds 0.0005 [14]. This makes it possible to neglect the terms containing h (denoted as $\ldots$ in the above expansion) and obtain the following approximate relation

$$\frac{1}{k^2} g(\delta^2 + \tau h) u \approx \frac{1}{k^2} g(\delta^2) u + h u = \frac{1}{k^2} \frac{\partial^2 u}{\partial z^2} + h u.$$

Substituting this approximation into the propagation operator, we obtain

$$P(L) = P\left(\frac{1}{k^2}\frac{\partial^2}{\partial z^2} + h\right) u \approx P\left(\frac{1}{k^2} g(\delta^2 + \tau h)\right) u.$$

Next, using Padé approximation (6) with new coefficients a_l' and b_l', we can write the following approximation of the propagation operator, that takes into account the inhomogeneous refractive index

$$P\left(\frac{1}{k^2} g(\xi)\right)\Big|_{\xi = \delta^2 + \tau h} u \approx \prod_{l=1}^{p} \frac{1 + a_l' \xi}{1 + b_l' \xi}\Bigg|_{\xi = \delta^2 + \tau h} u. \tag{7}$$

As a result, we come to a numerical scheme that is equivalent to the 2nd order one ($\alpha = 0$) except for coefficients a'_l and b'_l.

Note that the computational complexity of the proposed scheme is equal to the complexity of the 2nd order scheme. The difference is only in the Padé approximation coefficients. Approximation (7) simultaneously includes the differentiation operator, the square root operator, and the exponential operator. Thus, single approximation is responsible simultaneously for three parameters of the numerical scheme: grid steps Δx, Δz and the maximum propagation angle.

The idea of joint use of the Padé approximation for sampling along the longitudinal and transversal coordinates was expressed in the works [5,7]. However, previously it was limited to the case of a homogeneous medium. In this paper, we show that when the refractive index is sufficiently small, it is possible to generalize this idea to the case of an inhomogeneous medium without additional computational costs. A small refractive index just arises in the problems of tropospheric propagation. Of course, such a scheme is not applicable in the case of strong spatial variations of the refractive index. Latter occurs, for example, when modeling the water-ground boundary in hydroacoustics.

It should be noted the smallness of the refractive index is also significantly used in the derivation of the widely used SSF method, so this assumption is not a shortcoming compared to the SSF method. At the same time, the proposed scheme, as well as other finite-difference schemes, makes it possible to effectively model both the upper transparent boundary [19] and the lower impedance boundary [14].

It is recommended to use Padé approximations of the order $[p-1/p]$ or $[p-2/p]$ [14,19].

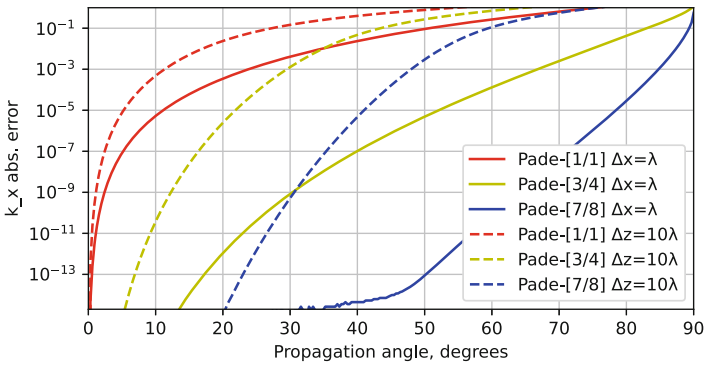


Fig. 1. Dependence of discrete dispersion relation error R on propagation angle θ. $\Delta z \to 0$.

Table 1. Optimal values of Δz for various PE numerical methods (larger is better). $\Delta x = 1\lambda$, rational approximation order is [7/8], acceptable error $tol = 10^{-3}$.

$\theta_{max}, ^\circ$	$\Delta z, \lambda$ (2nd order)	$\Delta z, \lambda$ (4th order)	$\Delta z, \lambda$ (joined)	$\Delta z, \lambda$ (SSF)
10	0.8	1.5	2.8	2.88
20	0.2	0.5	1.3	1.46
30	0.09	0.2	0.9	1.0
45	0.01	0.1	0.6	0.70
60	0.01	0.1	0.4	0.58
70	0.01	0.01	0.3	0.53

4 Numerical Results and Discussion

The first two subsections demonstrate the advantage of the proposed approach in terms of the maximum propagation angle and density of the computational grid. Then we demonstrate on a concrete example the consistency of the made assumption about the sufficient smallness of the refractive index. In the last example, we show the application of the proposed method in a realistic propagation scenario.

4.1 Error Analysis

In this section, we provide a discrete dispersion analysis [17,28] of the proposed scheme. The discrete horizontal wavenumber for the class of numerical schemes under consideration is written as follows [17]

$$k_x^d(\Delta x, \Delta z, a_1 \dots a_p, b_1 \dots b_p, \theta) = k + \frac{\ln \prod_{l=1}^{p} t_l}{i\Delta x},$$

$$t_l = \frac{1 - \frac{4a_l}{\tau}\left(\sin^2\left(\frac{k\Delta z \sin\theta}{2}\right) + 4\alpha \sin^4\left(\frac{k\Delta z \sin\theta}{2}\right)\right)}{1 - \frac{4b_l}{\tau}\left(\sin^2\left(\frac{k\Delta z \sin\theta}{2}\right) + 4\alpha \sin^4\left(\frac{k\Delta z \sin\theta}{2}\right)\right)},$$

where θ is the angle between the direction of the wave and the positive x direction.

The horizontal wavenumber for original one-way Helmholtz equation (1) is written as follows

$$k_x = \begin{cases} \sqrt{k^2 - k_z^2}, & |k_z| \le k, \\ i\sqrt{k_z^2 - k^2}, & |k_z| > k, \end{cases}$$

where $k_z = k \sin\theta$ is the vertical wavenumber.

Comparing the discrete and original dispersion relation

$$R\left(\Delta x, \Delta z, a_1 \dots a_p, b_1 \dots b_p, \theta\right) = \left|k_x^d\left(\Delta x, \Delta z, a_1 \dots a_p, b_1 \dots b_p, \theta\right) - k_x\left(k_z = k \sin\theta\right)\right|$$

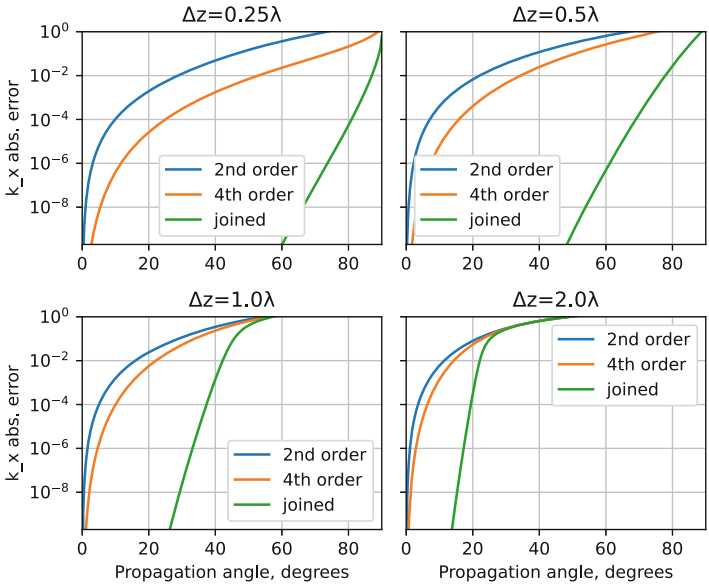


Fig. 2. Dependence of discrete dispersion relation error R on propagation angle θ. $\Delta x = 1\lambda$, Rational approximation order is equal to [7/8].

makes it possible to estimate the accuracy of a numerical scheme depending on its parameters [17]. Figure 1 demonstrates the dependence of discrete dispersion relation error R on propagation angle θ for the following three approximation orders: [1/1], [3/4], [7/8] and two values of longitudinal grid step Δx: 1.0λ and 10.0λ. In this example we set $\Delta z \to 0$, so the discretization by z is not considered. It is clearly seen that the accuracy monotonically decreases with increasing propagation angle. Increasing the order of rational approximation and decreasing grid step Δx gives a more accurate scheme. Thus, there is a direct dependency between the accuracy of the numerical scheme and the propagation angle.

Next, we consider the effect of the approximation of operator L on the accuracy of the numerical scheme. Figure 2 demonstrates the dependence of R on the propagation angle for the four different values of transversal grid step Δz: 0.25λ, 0.5λ, 1.0λ, 2.0λ and three variants of approximation by z: 2nd order, 4th order and the proposed joined approximation. Longitudinal grid step $\Delta x = 1.0\lambda$, Padé approximation order is [7/8]. It can be seen that, as before, the accuracy monotonically decreases with increasing propagation angle. It is also clearly observable how increasing the order of approximation by z increases the accuracy of the numerical scheme. At the same time, it should be noted that all three considered variants of approximation by z are computationally equivalent since they differ only in the coefficients of the scheme.

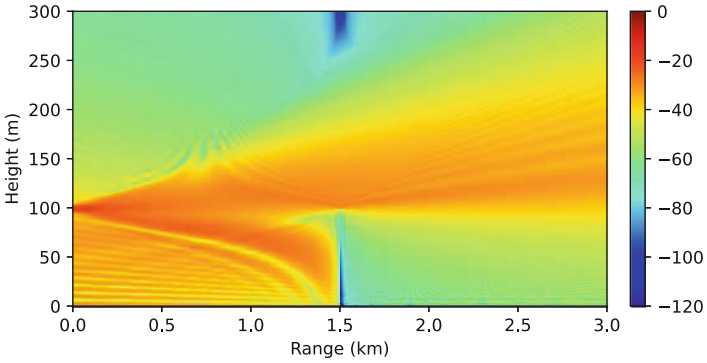


Fig. 3. Knife-edge diffraction. Two-dimensional distribution of the electromagnetic field ($20 \log |u(x, z)|$), obtained by the integral equation method [27]. Operational frequency is equal to 600 MHz.

Next, we will consider in more detail how the accuracy of the approximation by z affects the required density of the computational grid and, accordingly, the computational time. To determine the optimal density of the computational grid, we will solve the following maximization problem [17]

$$\Delta z \to \max$$

under condition

$$\max_{\theta \in [0, \theta_{max}]} R\left(\Delta x, \Delta z, a_1 \dots a_p, b_1 \dots b_p, \theta\right) < tol,$$

where θ_{max} is the maximum required propagation angle, tol is the acceptable error at each step.

For the SSF method, it is somewhat easier to determine the optimal Δz by using the Nyquist-Shannon sampling theorem

$$\Delta z \leq \frac{\lambda}{2 \sin \theta_{max}}.$$

Table 1 demonstrates the optimal values of Δz for several propagation angles and numerical methods. The acceptable error tol was taken equal to 10^{-3}. It can be seen that the proposed scheme allows the use of a much more sparse computational grid than other finite difference methods, and is almost equal to the SSF method by this criterion. The advantages of the proposed method are particularly visible on large propagation angles.

4.2 Knife-Edge Diffraction

In this subsection, we consider the classical knife-edge diffraction problem [21,27]. Here we also consider the backscattering from the obstacle. Modeling of

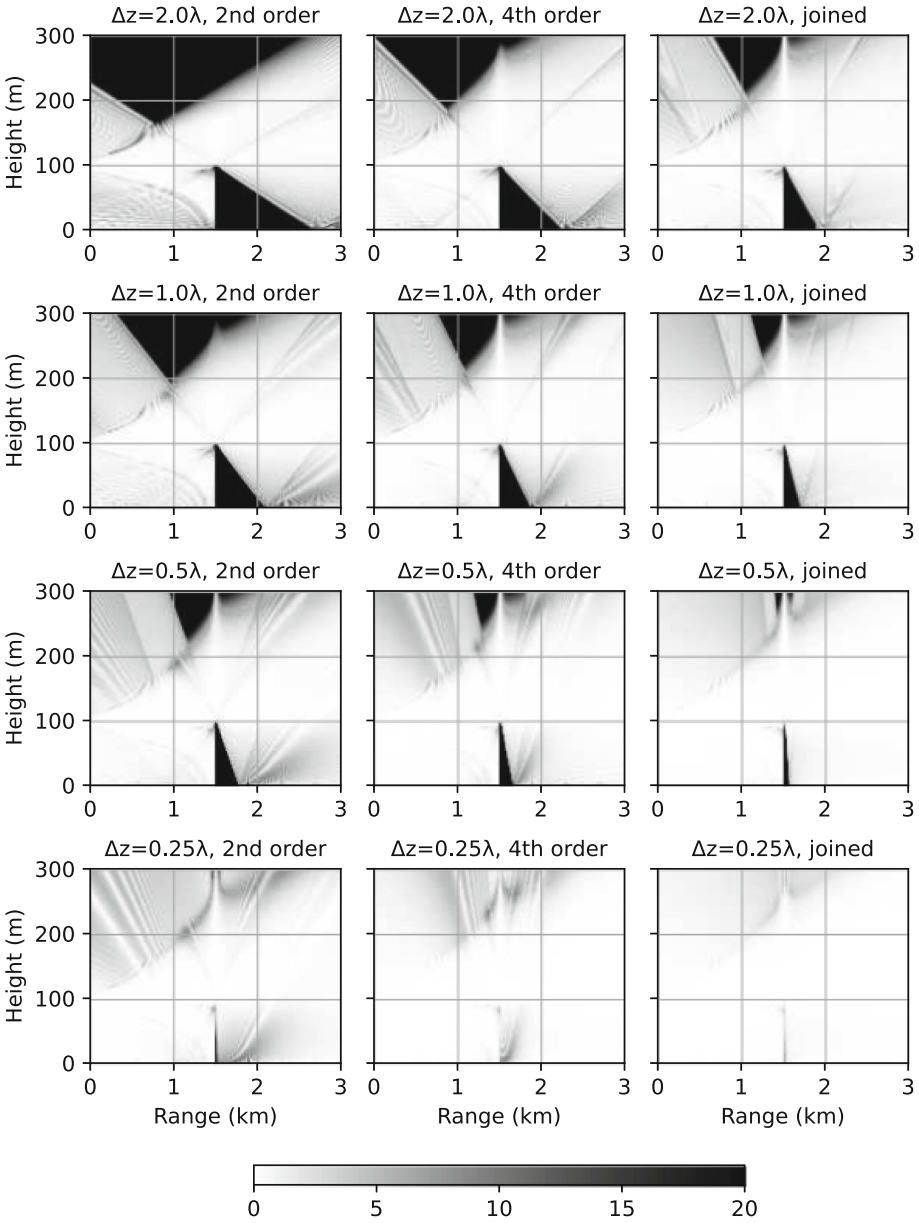


Fig. 4. Knife-edge diffraction. Two-dimensional distribution of the error between reference solution u_e and finite-difference solution u_{fd} ($|20\log|u_e(x,z)| - 20\log|u_{fd}(x,z)||$). In all examples, the order of the Padé approximation is equal to [7/8], longitudinal grid step $\Delta x = \lambda$.

diffraction on such obstacles at large propagation angles is essential when calculating the field in dense urban area. As a reference, we will use the solution obtained using the integral equation for the knife-edge diffraction [27]. The horizontally polarized monochromatic source is located at the height of 100 m over the perfectly conducted surface. The operation frequency is 600 MHz ($\lambda = 0.5$ m). Knife-edge with a height of 100 m is located at a distance of 1.5 km from the source of radiation. The reference solution is depicted in Fig. 3.

Figure 4 shows the spatial distribution of the error between the reference solution and the various configurations of the finite difference method. Padé approximation of order [7/8] with three various approximations by z and various values of Δz are considered. The backscattering from the knife-edge is modeled using the two-way PE approach [20]. It is clearly seen how the maximum propagation angle increases with increasing accuracy of the approximation. The need to handle large propagation angles when calculating the field in the diffraction zone behind the obstacle is clearly visible.

4.3 Propagation in a Duct

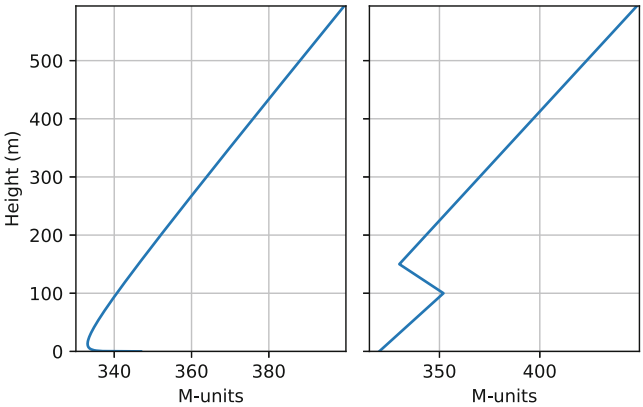


Fig. 5. M-profile of the evaporation duct (left) and elevated duct (right).

In this example, we model the radio-wave propagation in a tropospheric waveguide. The aim of this example is to demonstrate that the assumptions made in the previous section about the sufficient smallness of the tropospheric refractive index do not really affect the accuracy of the proposed method.

Modified refractivity m is determined by the refractive index of the troposphere n and the radius of the Earth R as follows

$$m = n + 1/R.$$

Function m makes it possible to take into account the over-the-horizon diffraction along with tropospheric refraction [14]. We further express the tropospheric refraction profile by the M-profile $M = 10^6(m-1)$. Figure 5 shows the tropospheric refractive index profiles for the two widely occurring waveguides: evaporated duct and elevated duct [14]. Figure 6 demonstrates the results of modeling in the mentioned profiles by the proposed method. The radiation frequency in this example is equal to 10 GHz ($\lambda = 0.03$ m). We will compare the results obtained in this example with the SSF method implemented in the PETOOL program [22]. Figure 7 shows the spatial distribution of the error between the proposed method and the SSF method. It can be seen that the results of both methods actually coincide. Thus, the proposed method can properly handle the inhomogeneities of the troposphere. It is also clear that the proposed method can properly handle the discrete transparent boundary condition [19], posed on the upper boundary of the computational domain.

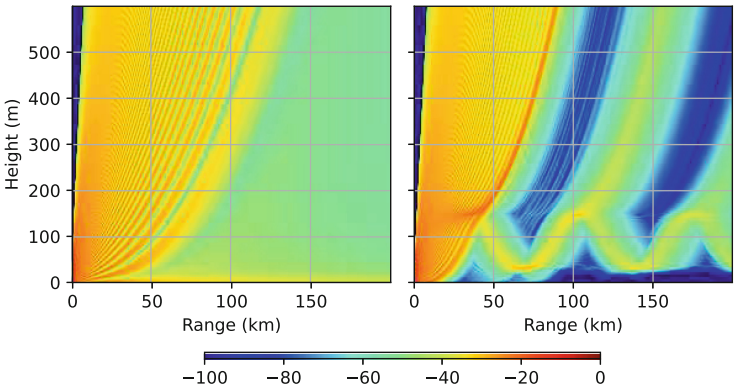


Fig. 6. Propagation in the evaporation duct (left) and elevated duct (right). Two-dimensional distribution of the electromagnetic field ($20\log|u(x,z)|$), obtained by the proposed method. In both examples, Padé approximation order is [7/8], $\Delta x = 1000\lambda$, $\Delta z = 0.5\lambda$. Operational frequency is equal to 10 GHz.

4.4 Propagation over Irregular Terrain

In the last example, we consider the propagation of radio-waves over irregular terrain in the elevated duct from the previous example. The radiation frequency in this example is equal to 1.5 GHz ($\lambda = 0.2$ m). Figure 8 shows the two-dimensional distribution of the electromagnetic field obtained by the proposed method with the following parameters: Padé approximation order in equal to [7/8], $\Delta x = 100\lambda$, $\Delta z = 3\lambda$. The inhomogeneities of the landscape are approximated by a piecewise constant function. Figure 9 and 10 show a comparison with

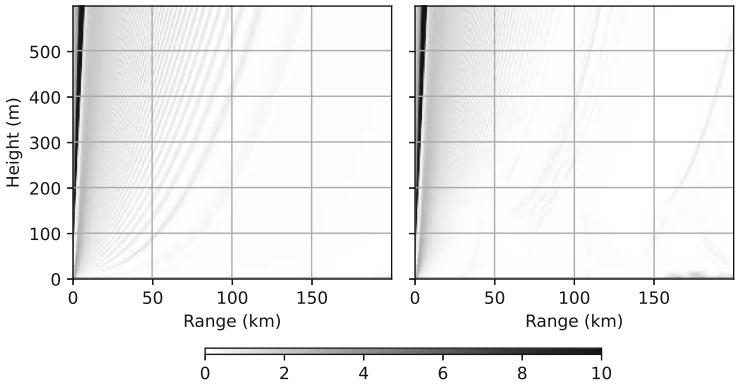


Fig. 7. Propagation in the evaporation duct (left) and elevated duct (right). Two-dimensional distribution of the error between reference solution u_{ssf}, obtained by the SSF method, and solution u_{fd}, obtained by the proposed method ($|20\log|u_{ssf}(x,z)| - 20\log|u_{fd}(x,z)||$).

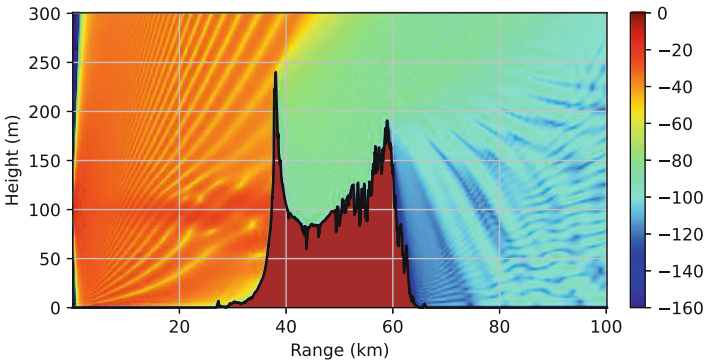


Fig. 8. Propagation in the elevated duct over irregular terrain. Two-dimensional distribution of the electromagnetic field ($20\log|u(x,z)|$), obtained by the proposed method. Operational frequency is equal to 1.5 GHz.

the 2nd order approximation. It is clearly seen that for the same computational parameters, the 2nd order scheme yields a significant underestimation of the field in the diffraction zone, as well as a noisy solution in several areas. To obtain a correct solution by the 2nd order scheme, it is necessary to use six times more dense grid by z.

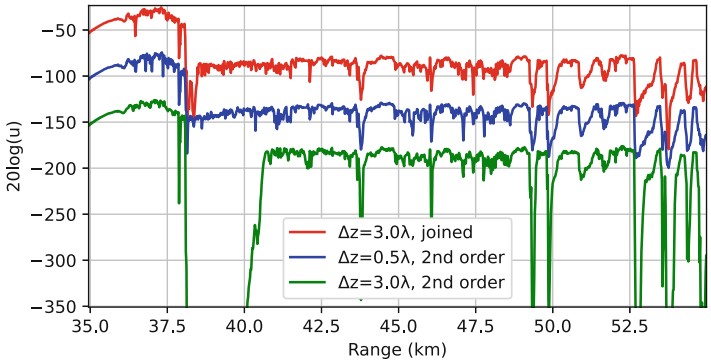


Fig. 9. Propagation in the elevated duct over irregular terrain. Distribution of the electromagnetic field $(20 \log |u(x, z)|)$ at the height of 5 m over the surface. The results are shifted by 50 dB for convenience.

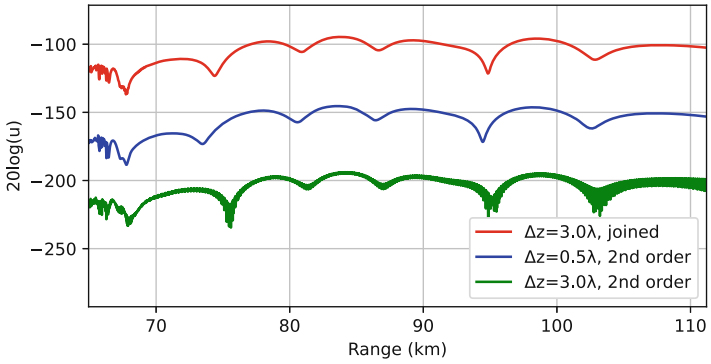


Fig. 10. Propagation in the elevated duct over irregular terrain. Distribution of the electromagnetic field $(20 \log |u(x, z)|)$ at the height of 5 m over the surface. The results are shifted by 50 dB for convenience.

5 Conclusion

The proposed method gives an opportunity to significantly improve the performance of finite-difference methods for solving PE in the inhomogeneous troposphere. At the same time, no significant changes to the existing software implementations are required, since the new scheme differs only in coefficients of the rational approximation. The new scheme retains all the advantages of the finite-difference schemes, in particular, the correct boundary conditions modeling. At the same time, the joint Padé approximation along the longitudinal and transversal coordinates made it possible to reduce the density of the computational grid and, accordingly, the computational time.

The proposed method is implemented as a Python 3 library and is freely available [15].

Acknowledgements. This study was supported by the Russian Science Foundation grant No. 21-71-00039.

References

1. Apaydin, G., Ozgun, O., Kuzuoglu, M., Sevgi, L.: A novel two-way finite-element parabolic equation groundwave propagation tool: tests with canonical structures and calibration. IEEE Trans. Geosci. Remote Sens. **49**(8), 2887–2899 (2011)
2. Baker, G.A., Graves-Morris, P.: Pade Approximants, vol. 59. Cambridge University Press, Cambridge (1996)
3. Brookner, E., Cornely, P.R., Lok, Y.F.: AREPS and TEMPER-getting familiar with these powerful propagation software tools. In: IEEE Radar Conference, pp. 1034–1043. IEEE (2007)
4. Cama-Pinto, D., et al.: Empirical model of radio wave propagation in the presence of vegetation inside greenhouses using regularized regressions. Sensors **20**(22), 6621 (2020)
5. Collins, M.D.: A split-step pade solution for the parabolic equation method. J. Acoust. Soc. Am. **93**(4), 1736–1742 (1993)
6. Collins, M.D., Siegmann, W.L.: Parabolic Wave Equations with Applications. Springer, New York (2019). https://doi.org/10.1007/978-1-4939-9934-7
7. Ehrhardt, M., Zisowsky, A.: Discrete non-local boundary conditions for split-step padé approximations of the one-way Helmholtz equation. J. Comput. Appl. Math. **200**(2), 471–490 (2007)
8. Fishman, L., McCoy, J.J.: Derivation and application of extended parabolic wave theories. I. The factorized Helmholtz equation. J. Math. Phys. **25**(2), 285–296 (1984)
9. Guo, Q., Long, Y.: Two-way parabolic equation method for radio propagation over rough sea surface. IEEE Trans. Antennas Propag. **68**, 4839–4847 (2020)
10. Guo, Q., Zhou, C., Long, Y.: Greene approximation wide-angle parabolic equation for radio propagation. IEEE Trans. Antennas Propag. **65**(11), 6048–6056 (2017)
11. Kuttler, J.R., Janaswamy, R.: Improved Fourier transform methods for solving the parabolic wave equation. Radio Sci. **37**(2), 1–11 (2002)
12. Lee, D., Schultz, M.H.: Numerical Ocean Acoustic Propagation in Three Dimensions. World Scientific, Singapore (1995)
13. Leontovich, M.A., Fock, V.A.: Solution of the problem of propagation of electromagnetic waves along the earth's surface by the method of parabolic equation. J. Phys. USSR **10**(1), 13–23 (1946)
14. Levy, M.F.: Parabolic Equation Methods for Electromagnetic Wave Propagation. The Institution of Electrical Engineers, UK (2000)
15. Lytaev, M.S.: Python wave prorogation library (2020). https://github.com/mikelytaev/wave-propagation
16. Lytaev, M., Borisov, E., Vladyko, A.: V2I propagation loss predictions in simplified urban environment: a two-way parabolic equation approach. Electronics **9**(12), 2011 (2020)
17. Lytaev, M.S.: Automated selection of the computational parameters for the higher-order parabolic equation numerical methods. In: Gervasi, O., et al. (eds.) ICCSA 2020. LNCS, vol. 12249, pp. 296–311. Springer, Cham (2020). https://doi.org/10.1007/978-3-030-58799-4_22

18. Lytaev, M.S.: Numerov-pade scheme for the one-way Helmholtz equation in tropospheric radio-wave propagation. IEEE Antennas Wirel. Propag. Lett. **19**(12), 2167–2171 (2020)
19. Lytaev, M.S.: Nonlocal boundary conditions for split-step padé approximations of the Helmholtz equation with modified refractive index. IEEE Antennas Wirel. Propag. Lett. **17**(8), 1561–1565 (2018)
20. Mills, M.J., Collins, M.D., Lingevitch, J.F.: Two-way parabolic equation techniques for diffraction and scattering problems. Wave Motion **31**(2), 173–180 (2000)
21. Nguyen, V.D., Phan, H., Mansour, A., Coatanhay, A., Marsault, T.: On the proof of recursive Vogler algorithm for multiple knife-edge diffraction. IEEE Trans. Antennas Propag. **69**(6), 3617–3622 (2020)
22. Ozgun, O., et al.: PETOOL v2.0: parabolic equation toolbox with evaporation duct models and real environment data. Comput. Phys. Commun. **256**, 107454 (2020)
23. Permyakov, V.A., Mikhailov, M.S., Malevich, E.S.: Analysis of propagation of electromagnetic waves in difficult conditions by the parabolic equation method. IEEE Trans. Antennas Propag. **67**(4), 2167–2175 (2019)
24. Ramos, G.L., Pereira, P.T., Leonor, N., Caldeirinha, F.R.: Analysis of radiowave propagation in forest media using the parabolic equation. In: 2020 14th European Conference on Antennas and Propagation (EuCAP). IEEE (2020)
25. Samarskii, A.A., Mikhailov, A.P.: Principles of Mathematical Modelling: Ideas, Methods, Examples. Taylor and Francis, Routledge (2002)
26. Taylor, M.: Pseudodifferential Operators and Nonlinear PDE, vol. 100. Springer, Cham (2012). https://doi.org/10.1007/978-1-4612-0431-2
27. Vavilov, S.A., Lytaev, M.S.: Modeling equation for multiple knife-edge diffraction. IEEE Trans. Antennas Propag. **68**(5), 3869–3877 (2020)
28. Wang, D.D., Pu, Y.R., Xi, X.L., Zhou, L.L.: An analysis of narrow-angle and wide-angle shift-map parabolic equations. IEEE Trans. Antennas Propag. **68**(5), 3911–3918 (2020)
29. Zhang, P., Bai, L., Wu, Z., Guo, L.: Applying the parabolic equation to tropospheric groundwave propagation: a review of recent achievements and significant milestones. IEEE Antennas Propag. Mag **58**(3), 31–44 (2016)